

# In-situ Laser Pulse Characterization using Photoelectrons

Michael Hemsworth

*Department of Physics and Astronomy, University of British Columbia*  
December 18, 2021

## Abstract

The time resolved method of pump-probe spectroscopy, in particular time-resolved angle-resolved photoelectron spectroscopy (TR-ARPES), plays an important role in the exploration of ultrafast electronic dynamics, such as electron-phonon coupling, in condensed matter systems. For such experiments, it is important to fully characterize the laser pulses used to both excite and probe the sample. In this report, we explore the viability of different pulse measurement techniques as they relate to TR-ARPES, and propose a general approach to perform such measurements in-situ using a known sample and its resulting photoelectron spectrum.

## 1 Introduction

Pump-probe spectroscopy is a powerful tool utilized to study ultrafast (10-1000 femtoseconds) electron dynamics. In this technique, an ultrafast pump pulse first promotes the system into an excited state of interest. A time-delayed ultrafast probe pulse is then used to project the excited state dynamics onto a final state observable. The time delay between the pump and probe pulses is then varied to acquire several snapshots in time that paint a picture of the overall dynamics. Many different probing schemes exist with different final state projections, each with their own advantages and disadvantages. Of those schemes, time-resolved angle-resolved photoelectron spectroscopy (TR-ARPES) has proven to be a powerful tool to study condensed matter systems and their dynamics [1, 2]. In particular, TR-ARPES has demonstrated its usefulness in interrogating electron-phonon interactions, such as the relaxation channels of hot electronic distributions [3], superconducting gap dynamics of cuprate superconductors [4], dynamics in bulk FeSe [5], and surface-state dynamics in topological materials [6].

In a TR-ARPES experiment, the photon energy of the pump is typically in the 1 eV range to match

the gap between the conduction and valence bands of interest. The photon energy of the probe pulse is chosen to be much higher than the work function of the material to eject free electrons into the vacuum with sufficient kinetic energy to utilise the sudden approximation. In this limit, the ionization process is assumed to be sudden, with no post-collisional interaction between the photoelectron and the system it leaves behind. Further details can be found in Ref. [7]. Since the work function of most materials lies within the 3-6 eV range, the probe pulse energy should be at least  $\geq 6$  eV.

Generally, "well-known" ultrafast laser pulses are used to interrogate unknown condensed matter systems. However, it is quite often the case that one or both of the pulses are not fully characterized. This is due to the lack of characterization methods at higher photon energies (in particular for the probe pulse), as well as the difficulty setting up elaborate diagnostics in the ultra high vacuum conditions required for TR-ARPES. As more elaborate high photon energy sources are developed, accurate pulse characterization becomes more important.

We can overcome these limitations and fully characterize both pulses by performing an in-situ measurement. If we start with a system that is well understood (i.e can be accurately described theoretically), then full characterization of the pump and probe laser pulses is possible. This would enable more accurate time resolution in current experiments, as well as open the door for more complex pulses to be used in the study of e.g. lightwave electronics [8]. The rest of this paper will briefly introduce the mathematics of laser pulses and how they are measured, followed by an exploration of characterization techniques that may be useful in the context of TR-ARPES experiments.

## 2 TR-ARPES Experimental Setup

A typical TR-ARPES experiment consists of three main components, the laser source, the experimen-

tal chamber, and the electron analyzer. The laser source generates two ultrafast laser pulses (the pump and the probe) from the same seed laser to ensure they are stable with respect to each other. The probe pulse has a variable time delay to allow for time resolved measurement. The pulses then pass through a window into the experimental chamber, which holds the sample of interest. The pump excites the sample, followed by the probe that ionizes the excited state, generating free electrons. The free electrons are then collected by the electron analyzer which measures the electron kinetic energy and angle of ejection. The experimental chamber and electron analyzer must be kept under ultra-high vacuum conditions so that the electrons have a free path to the detector without any particle collisions in between.

### 3 Laser Pulses

An ultrafast laser pulse is comprised of a coherent superposition of many different frequency components. When all frequency components are maximally in phase, they constructively interfere inside the pulse and destructively interfere everywhere else. The pulse duration is directly related to the number of frequency components, also called the bandwidth of the pulse. The larger the bandwidth, the shorter the pulse can be. This is a direct result of the Fourier transform, and we say that a pulse is "transform limited" if its duration matches the shortest possible duration supported by the bandwidth. If the frequency components are not maximally in phase, the pulse duration will lengthen with different frequencies arriving at different times during the pulse. This is called "chirp" and a simple example of a linear chirp is shown in Fig. 1. Much more complex chirps are possible which can have dramatic effects on both the pulse shape and duration.

The electric field as a function of time of an ultrafast laser pulse can be fully represented by

$$E(t) = A(t) \exp(i\omega_0 t - \phi(t)), \quad (1)$$

where  $A(t)$  is the time-dependent amplitude,  $\omega_0$  is the carrier frequency and  $\phi(t)$  is the time-dependent phase. Equivalently, the pulse can also be represented in the frequency domain via a Fourier Transform

$$\tilde{E}(\omega) = \tilde{A}(\omega) \exp(-i\tilde{\phi}(\omega)), \quad (2)$$

where  $\tilde{A}(\omega)$  is the spectral amplitude and  $\tilde{\phi}(\omega)$  is the spectral phase. The spectral phase is Taylor

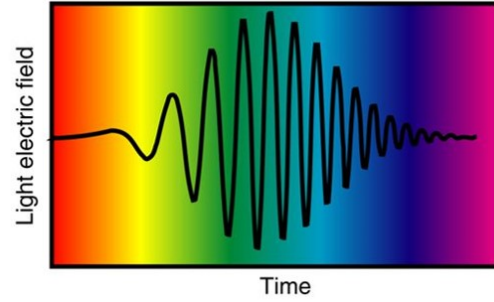


Figure 1: Representation of a linearly chirped pulse. We can see that the lower ("red") frequency components arrive before the higher ("blue") frequency components. Taken from [9].

expanded about the carrier frequency  $\omega_0$ , where the linear term is the group velocity and describes a time shift, the second order term is called the group velocity dispersion (GVD), the third order term is called third order dispersion (TOD) and higher order terms are lumped together as higher order dispersion (HOD). Different media will have varying strengths of these dispersion parameters, which determine the frequency-dependent speed of light in the medium. Propagating a pulse through a medium (such as a window into the experimental chamber) is equivalent to multiplying the spectral representation of the pulse by the material's transfer function

$$H(\omega) = B(\omega) e^{i\phi_H(\omega)}, \quad (3)$$

where  $B(\omega)$  is the amplitude of the transfer function (related to material absorption) and  $\phi_H(\omega)$  is the spectral phase of the material. The amplitude is often ignored such that multiplying by the transfer function simply adds the spectral phase of the medium to the phase of the initial pulse described by Eq. 2.

The key takeaway here is that all materials in the laser path (including air) can affect pulse shape and duration, sometimes in very complicated ways. It is therefore very important to verify that the laser pulses used in experiments are preparing the correct states, and that they are short enough to temporally resolve the dynamics of interest.

### 4 Pulse Measurement

Noting that optical frequencies are much higher than the bandwidth of modern electronics, direct time domain measurements are impractical. Therefore the vast majority of measurements are made in the frequency domain using spectrometers.

Since we can only measure intensity ( $I(t) = |E(t)|^2$  or  $S(\omega) = |\tilde{E}(\omega)|^2$ ) and not the field directly, the phase information is lost unless we measure some interference between two fields. Without the phase we cannot accurately measure important parameters like pulse duration and chirp. Therefore a nonlinear process that depends on the square (or higher powers) of the electric field must be used to retrieve the phase.

#### 4.1 Frequency Resolved Optical Gating

The standard method for full pulse characterization (amplitude and phase) is called frequency resolved optical gating (FROG) [10]. The basic premise of FROG is to generate a 2D spectrogram (intensity vs. time and frequency) by correlating the input pulse with a gate pulse in a nonlinear medium. The nonlinear medium mixes the two pulses and creates a new signal pulse which encodes both the amplitude and phase information. The correlation is performed by scanning the gate pulse through the input pulse and measuring the resulting spectrum as a function of time delay. The mathematical description of the FROG spectrogram  $S_{FROG}(\omega, \tau)$  is

$$S_{FROG}(\omega, \tau) = \left| \int_{-\infty}^{\infty} E_{sig}(t, \tau) e^{i\omega t} dt \right|^2, \quad (4)$$

where  $E_{sig}(t, \tau)$  is the signal pulse that depends on both the input pulse and the gate pulse with delay  $\tau$ . Many different nonlinear mixing schemes can be used in FROG, the simplest case being second harmonic generation (SHG FROG). In SHG FROG  $E_{sig}(t, \tau) = E(t)E(t - \tau)$ , where the gate pulse is a replica of the input pulse.

Figure 2 shows a typical schematic of an SHG FROG pulse measurement device. The pulse to be measured is first split into two identical copies by a beamsplitter, which are later recombined at a small crossing angle in a nonlinear crystal. A translation stage in one arm of the FROG allows one of the replica pulses to be delayed with respect to the other. When the pulses overlap in both space and time in the crystal, they mix in a second order nonlinear process, generating a new pulse at the second harmonic (SH) frequency of the input pulse. The SH pulse is then measured with a spectrometer at several different time delays and the resulting 2D spectrogram is passed through an algorithm that uniquely reconstructs the electric field (both amplitude and phase) of the input pulse. Figure 3 shows

an example of FROG spectrograms for different linearly chirped pulses. In this simple example, one can see directly that the tilt in the spectrogram directly maps to the chirp in the pulse. For a quantitative assessment of the pulse or for more complex pulses, the spectrogram would be fed into an algorithm that retrieves the pulse amplitude and phase.

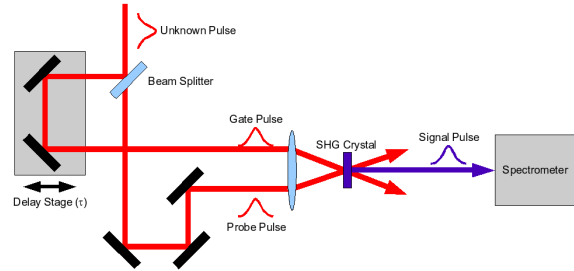


Figure 2: Schematic of a SHG FROG device. An unknown input pulse is split into two replicas, one being time delayed with respect to the other using a variable delay stage. The pulses are then mixed in a nonlinear medium that generates the signal pulse at double the frequency, which is then measured by a spectrometer at each time delay.

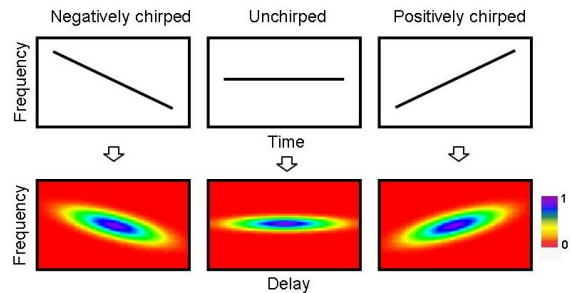


Figure 3: FROG spectrograms for different linearly chirped pulses. One can see that the tilt in the spectrogram directly maps to the chirp of the pulse. The spectrograms would be fed through a retrieval algorithm to obtain the electric field of the laser pulse. Color axis is a normalized intensity. Taken from [9].

In the context of measuring pulses used in TR-ARPES experiments, FROG has two main limitations. First, the probe photon energies are typically in the vacuum/extreme ultraviolet (VUV/XUV). At these photon energies there are no suitable nonlinear crystals to generate a FROG signal. Second, material dispersion is also very strong at these photon energies. Transmitting pulses through beam-splitters, glass windows etc. will strongly chirp the pulses. Therefore having a separate diagnostic beam path from that of the sample in the experimental chamber may lead to inaccurate pulse mea-

measurements. There are other methods of pulse characterization utilizing photoelectrons as the spectrogram signal, which are more naturally suited to TR-ARPES. Some of these techniques will be explored in the next sections.

## 4.2 Photoelectron Pulse Characterization

In the field of attosecond laser physics, a common pulse characterization technique is attosecond streaking [11]. It uses an extremely short attosecond XUV pulse to eject electrons from a gas target in the presence of a much longer infrared (IR) dressing field. The IR field is strong enough such that the free electrons are accelerated, but weak enough that no strong field ionization of the gas target occurs from the IR alone. In this way the photoelectron spectrum is modulated by the IR field as a function of delay between the two pulses. The resulting spectrogram traces exactly the vector potential of the IR field and its time derivative gives the electric field. Figure 4 shows an example of an attosecond streaking spectrogram in argon.

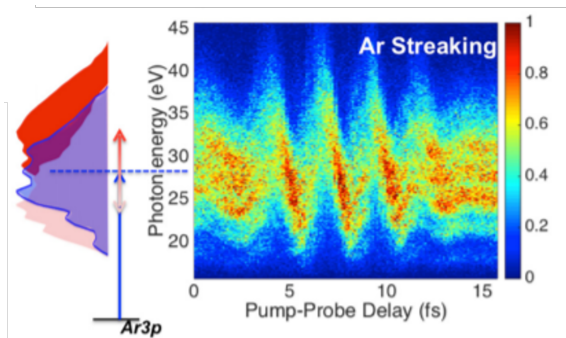


Figure 4: Spectrogram of an attosecond streaking measurement in argon. The spectrogram traces exactly the vector potential of the IR dressing field. Taken from [12].

Attosecond streaking is also possible in solids [13], however it is not particularly suitable for TR-ARPES experiments. It is conditional on short XUV pulses, which by the Fourier transform limit necessitates a large bandwidth. Resolving band structures then becomes an issue.

## 4.3 General Photoelectron FROG for TR-ARPES

In principle, if the material is well described system, the electric field of the laser pulses should be retrievable from the photoelectron spectrum. The following is a basic overview of how that could be achieved.

We are looking to calculate the transition probability  $w_{fmi}$  of a two-photon excitation that results in a free electron. We start with an  $N$ -electron ground state  $\Psi_i^N$  and one of the possible final states  $\Psi_f^N$  via an intermediate state  $\Psi_m^N$ . The transition probability will be proportional to the square of the transition matrix elements

$$w_{fmi}(t, \tau) \propto \left| \left\langle \Psi_f^N | H_{int}^{(2)}(t - \tau) | \Psi_m^N \right\rangle \cdot \left\langle \Psi_m^N | H_{int}^{(1)}(t) | \Psi_i^N \right\rangle \right|^2 \cdot \delta(E_f^N - E_i^N - h\nu_1 - h\nu_2), \quad (5)$$

where  $H_{int}^{(j)}(t)$  is the perturbative Hamiltonian for the interaction with a photon from the  $j^{\text{th}}$  laser pulse.  $H_{int}$  is given by

$$H_{int}(t) = \frac{e}{2mc} (\mathbf{A}(t) \cdot \mathbf{p} + \mathbf{p} \cdot \mathbf{A}(t)) = \frac{e}{mc} \mathbf{A}(t) \cdot \mathbf{p}, \quad (6)$$

where  $\mathbf{p}$  is the electronic momentum and  $\mathbf{A}$  is the laser vector potential. Note that in Eq. 6 the scalar potential was chosen to be  $\Phi = 0$ , the second order term in  $\mathbf{A}$  was dropped, and the dipole approximation was used to allow the commutation of  $\mathbf{A}$  and  $\mathbf{p}$  [7]. We can use Eq. 5 to write the equation for a photoelectron spectrogram with a similar form to Eq. 4

$$S(\omega, \tau) \propto \sum_{f,m,i} \left| \int_{-\infty}^{\infty} w_{fmi}(t, \tau) e^{i\omega t} dt \right|^2. \quad (7)$$

The kinetic energy of the emitted photoelectrons is given by

$$E_{kin} = h\nu_1 + h\nu_2 - (\phi + |E_B|), \quad (8)$$

where  $h\nu_j$  is the photon energy of pulse  $j$ ,  $\phi$  is the work function of the material and  $E_B$  is the binding energy of the electron inside the material. From Eqs. 7 and 8, the full electric fields should be reconstructible from the photoelectron spectrogram in the same way as a standard FROG spectrogram except with an energy shift of  $-(\phi + |E_B|)$ . The transition probability is dependent on the dynamics of the system, so a non-resonant excitation to a virtual intermediate state is preferred. Since a virtual state has zero lifetime, the photoelectron signal would only be present when both laser pulses are overlapped in time, thus simplifying the analysis significantly.

## 5 Conclusion

In the context of pump-probe experiments, it is of critical importance to well-characterize the laser pulses used to both excite and probe the system of interest. In this paper we discussed ultrafast laser pulses, their characteristics and how to measure them. FROG is the most common option for pulse characterization, but it has limits in the range of accessible photon energies. In-situ methods that leverage the photoelectron spectra generated by e.g. TR-ARPES should in principle be possible, provided the condensed matter system is well understood theoretically.

## References

- [1] M. X. Na, A. K. Mills, F. Boschini, M. Michiardi, B. Nosarzewski, R. P. Day, E. Razzoli, A. Sheyerman, M. Schneider, G. Levy, S. Zhdanovich, T. P. Devereaux, A. F. Kemper, D. J. Jones, and A. Damascelli. Direct determination of mode-projected electron-phonon coupling in the time domain. *Science*, 366(6470):1231–1236, 2019.
- [2] Umberto De Giovannini, Hannes Hübener, Shunsuke A. Sato, and Angel Rubio. Direct measurement of electron-phonon coupling with time-resolved arpes. *Phys. Rev. Lett.*, 125:136401, Sep 2020.
- [3] L Perfetti, P A Loukakos, M Lisowski, U Bovenstiepen, M Wolf, H Berger, S Biermann, and A Georges. Femtosecond dynamics of electronic states in the mott insulator 1t-TaS<sub>2</sub> by time resolved photoelectron spectroscopy. *New Journal of Physics*, 10(5):053019, may 2008.
- [4] Christopher L Smallwood, James P Hinton, Christopher Jozwiak, Wentao Zhang, Jake D Koralek, Hiroshi Eisaki, Dung-Hai Lee, Joseph Orenstein, and Alessandra Lanzara. Tracking cooper pairs in a cuprate superconductor by ultrafast angle-resolved photoemission. *Science*, 336(6085):1137–1139, June 2012.
- [5] S. Gerber, S.-L. Yang, D. Zhu, H. Soifer, J. A. Sobota, S. Rebec, J. J. Lee, T. Jia, B. Moritz, C. Jia, A. Gauthier, Y. Li, D. Leuenberger, Y. Zhang, L. Chaix, W. Li, H. Jang, J.-S. Lee, M. Yi, G. L. Dakovski, S. Song, J. M. Glowonia, S. Nelson, K. W. Kim, Y.-D. Chuang, Z. Hussain, R. G. Moore, T. P. Devereaux, W.-S. Lee, P. S. Kirchmann, and Z.-X. Shen. Femtosecond electron-phonon lock-in by photoemission and x-ray free-electron laser. *Science*, 357(6346):71–75, 2017.
- [6] J. A. Sobota, S. Yang, J. G. Analytis, Y. L. Chen, I. R. Fisher, P. S. Kirchmann, and Z.-X. Shen. Ultrafast optical excitation of a persistent surface-state population in the topological insulator bi<sub>2</sub>se<sub>3</sub>. *Phys. Rev. Lett.*, 108:117403, Mar 2012.
- [7] Andrea Damascelli. Probing the electronic structure of complex systems by ARPES. *Physica Scripta*, T109:61, 2004.
- [8] J. Reimann, S. Schlauderer, C. P. Schmid, F. Langer, S. Baierl, K. A. Kokh, O. E. Tereshchenko, A. Kimura, C. Lange, J. Güdde, U. Höfer, and R. Huber. Subcycle observation of lightwave-driven dirac currents in a topological surface band. *Nature*, 562(7727):396–400, Oct 2018.
- [9] Rick Trebino. Georgia institute of technology ultrafast optics group.
- [10] Rick Trebino, Kenneth W. DeLong, David N. Fittinghoff, John N. Sweetser, Marco A. Krumbügel, Bruce A. Richman, and Daniel J. Kane. Measuring ultrashort laser pulses in the time-frequency domain using frequency-resolved optical gating. *Review of Scientific Instruments*, 68(9):3277–3295, 1997.
- [11] J. Itatani, F. Quéré, G. L. Yudin, M. Yu. Ivanov, F. Krausz, and P. B. Corkum. Attosecond streak camera. *Phys. Rev. Lett.*, 88:173903, Apr 2002.
- [12] L. Cattaneo, J. Vos, M. Lucchini, L. Gallmann, C. Cirelli, and U. Keller. Comparison of attosecond streaking and rabbitt. *Opt. Express*, 24(25):29060–29076, Dec 2016.
- [13] Michael Krüger, Markus Schenk, and Peter Hommelhoff. Attosecond control of electrons emitted from a nanoscale metal tip. *Nature*, 475(7354):78–81, July 2011.